Materials Today • Volume xxx, Number xx • xxxx 2020 RESEARCH

ELSEVIER

RESEARCH: Original Research

All-in-one 3D acceleration sensor based on coded liquid–metal triboelectric nanogenerator for vehicle restraint system

Binbin Zhang [1,2,†], Zhiyi Wu [1,†], Zhiming Lin [1,4,†], Hengyu Guo [1], Fengjun Chun [2], Weiqing Yang [2], Zhong Lin Wang [1,3,*]

[1] Beijing Institute of Nanoenergy and Nanosystems, Chinese Academy of Sciences, Beijing, China
[2] Key Laboratory of Advanced Technologies of Materials (Ministry of Education), School of Materials Science and Engineering, Southwest Jiaotong University, Chengdu 610031, China
[3] School of Materials Science and Engineering, Georgia Institute of Technology, Atlanta, GA 30332, USA
[4] College of Electronic and Information Engineering, Southwest University, Chongqing 400715, China

Vehicle restraint systems play an irreplaceable role to limit passenger injuries when an accident occurs, in which, the 3D acceleration sensor (AS) is an essential component to detect the collision position and force. However, there are some defects for commercial sensors such as passive sensing, low sensitivity and high manufacturing cost. Here, we report a lightweight, high-sensitivity, low-cost and self-powered 3D AS based on a liquid–metal triboelectric nanogenerator (LM-TENG). In view of the coded strategy of the electrodes, the 3D AS retains the smallest size, lowest weight and highest integration compared to the currently reported self-powered AS. The fabricated sensor possesses wide detection range from 0 to 100 m/s^2 in the horizontal direction and 0 to 50 m/s^2 in the vertical direction at a sensitivity of 800 mV/g. The open-circuit voltage shows a negligible decrease after continuously operating for 100,000 times, showing excellent stability and durability. Furthermore, the 3D AS is demonstrated as a part of the airbag system to spot the collision position and force of the car simultaneously. This work will further promote the commercialization of TENG-based sensor and exhibits a prospective application in the vehicle restraint system.

Introduction

In the traffic field, the safety of passengers is protected by the vehicle crashworthiness, in which, the vehicle structure and restraint system are both the key elements [1–3]. For vehicle restraint systems, the 3D acceleration sensors are the indispensable component that can provide pivotal information to the electronic controller unit when the collision happened, such as collision position and force [4]. However, there are some limitations of commercial acceleration sensors which can be mainly classified into three types including piezoresistive, capacity and piezoelectric type. For example, the piezoresistive and capacity acceleration sensors always need the extra power supply, thus increasing the power consumption and shorten the operation period [5]. Although the piezoelectric type is self-powered, the electric output of which is small and could be influenced by the environmental noise as well as requiring high precision measurement system [6,7]. Consequently, it is necessary to develop a new type of acceleration sensor with high sensitivity and can actively generate electric signals as a response to the acceleration.

Recently, the triboelectric nanogenerator (TENG) invented by Wang's group in 2012, based on a coupling effect of contact electrification and electrostatic induction, has been proved as an efficient approach to convert mechanical energy to electricity, which has comprehensive applications in the ambient energy harvesting (wind, ocean wave, human, etc.) and high sensitive

* Corresponding author.
E-mail address: Wang, Z.L. (zhong.wang@mse.gatech.edu)
† These authors contributed equally to this work.

 https://doi.org/10.1016/j.mattod.2020.10.031

Please cite this article in press as: B. Zhang et al., Materials Today (2020), https://doi.org/10.1016/j.mattod.2020.10.031

self-powered sensing systems [8–14]. Mainly utilizing the triboelectrification between the conventional polymer film and the other materials, the TENG based active sensors have shown extremely high sensitivity to ambient mechanical stimulus [15–18]. Moreover, featured as lightweight, cost-effective, shape adjustable as well as high efficiency, the TENG is able to be designed into various structures to meet the diverse demands of sensing in daily life. Various self-powered active sensors based on TENG have been developed such as traffic volume sensors [19], auditory sensors [20], tactile sensors [21], gas sensors [22], smart keyboards [23], angle sensors [24] and so on. In real life, the acceleration sensor, especially 3D acceleration sensor, plays a critical role in many fields, such as earthquake detect, vehicle restraint system, human–machine interaction and so on [25]. Although the acceleration sensors based on TENG have been reported since 2014, the small detection range, large size and weight block their commercial applications, as shown in Table S1. In previous works, liquid metal has been proven to be an excellent material for TENG, with a high energy conversion efficiency of 70.6%, indicating a potential approach for fabricating high-sensitivity and small-sized self-powered sensors [26–28].

Here, we report a small-sized, lightweight, high-sensitivity and self-powered 3D AS based on liquid metal triboelectric nanogenerator (LM-TENG). The performance of the acceleration sensor is systematically studied both theoretically and experimentally. The acceleration sensor shows broad acceleration response (0–50 m/s^2 in the vertical direction and 0–100 m/s^2 in the horizontal direction) and high sensitivity (800 mV/g), ascribing to the large surface area of nanowires modified polytetrafluoroethylene (n-PTFE) and high energy conversion efficiency of liquid metal. The sensor possesses a cylindrical structure (28.75 mm in diameter and 7.22 mm in height) and a weight of 3.63 g. The open-circuit voltage shows a negligible decrease over 100 000 cycles, evidently presenting excellent stability. The length of the coded electrodes is designed to adjust to the volume of the liquid metal droplet, as a result, the accuracy of direction identification is significantly enhanced. Compared to recently reported works, the 3D acceleration sensor retains the smallest size, lowest weight, highest detection range, highest integration and excellent stability, as shown in Table S1. In addition, the 3D AS is demonstrated as a part of the vehicle safety restraint system to detect the collision position and force of the car to protect the safety of occupants. This study further expands the commercial application of TENG as self-powered sensors in transportation field.

Results and discussion

An exploded view schematic illustration highlights various aspects of the layer-by-layer structure of the 3D AS based on LM-TENG, as shown in Fig. 1a. A concave surface with a slop angle of nearly 5 degrees is fabricated on one acrylic plate by the laser cutter to be the substrate of the mercury droplet. The cross-section view of the concave-shaped substrate is displayed in Fig. S1a and b. On the other side of the acrylic plate, four coded and one annular copper electrodes are deposited, with a thickness of 200 nm, which were utilized to detect the direction and acceleration in the horizontal direction. The coded strategy and the digital photograph of the electrodes are illustrated in Fig. 1g and h, where the width of the electrodes is 1 mm and the distance between the neighboring electrodes is 0.5 mm. Silver electrodes are connected with the copper electrodes correspondingly as the test electrodes, as illustrated in Fig. 1f. It is worth to be noted that the silver electrodes and copper electrodes are separated by an acrylic plate with several hole channels to reduce the noise influenced by the test electrodes. A Kapton film is attached to the silver electrodes to protect it from the influence of water and dust from the ambient environment. An acrylic ring is attached to the concave-shaped substrate to limit the movement of the mercury droplet. On the top of the ring, a layer of copper-coated PTFE film is laminated as one of the triboelectric layers. The cross section view of the whole device is shown in Fig. S1c. As shown in Fig. 1j, the nanowires structure is created on the PTFE surface to enhance the surface charge density and output of the sensor [29,30]. The detailed fabrication process is schematically illustrated in Supporting Fig. S2. The fabricated 3D AS possesses a cylindrical structure (28.75 mm in diameter and 7.22 mm in height) and a weight of 3.63 g, as displayed in Fig. 1i and S3.

The basic principle of the 3D AS can be elucidated from two aspects, movement in the vertical direction and in the horizontal direction. As demonstrated in Fig. 1b, at the original state, when the mercury droplet is brought to contact with the PTFE film, ascribing to the difference of the electron affinity between the two, the electrons transfer from the mercury surface to the PTFE surface, as a result, the PTFE film is negatively charged and the mercury is positively charged. The triboelectric charges cannot be conducted or neutralized for a period of time. At this moment, the positive tribo-charges are fully compensated with the opposite ones, consequently, there is no electric output generated on the electrode. Once the droplet moves down forward and separates with the PTFE film, the equilibration of the electric field is broken, the potential difference will create a flow of electrons from the copper electrode to the ground to equilibrate the potential until a new electric equilibrium is established (droplet moved to the lowest point). Then, the droplet moves up forward, the electrons flow from the ground to the copper electrode until the initial state. The static and dynamic potential distribution of mercury droplet and PTFE film upon contact and separation is simulated by COMSOL, as illustrated in Fig. 1c and Supporting Movie 1. When the droplet moves in the horizontal direction, the electric equilibrium establishes at the third state, in other words, the droplet moved directly to the top of the electrode. Otherwise, there are electrons flowing from the electrode to the ground or the opposite, as displayed in Fig. 1d. As clearly shown in Fig. 1e and Supporting Movie 2, the static and dynamic potential distribution when the droplet moves from the inner electrode (E1) to the outer electrode (E4) is calculated *via* COMSOL.

Materials selection plays a critical role in the structure design and electric output of the sensor based on TENG. For the triboelectric layer, we fabricated the nanowires on the surface of PTFE film and the optimized dimension was obtained, as shown in Fig. S4. In this work, the material selection of the moving part is very important, which has an influence on the sensitivity, detection range, stability as well as the degree of integration of the sensor. As shown in Fig. 2a, mercury, water droplet, and PTFE

Please cite this article in press as: B. Zhang et al., Materials Today (2020), https://doi.org/10.1016/j.mattod.2020.10.031

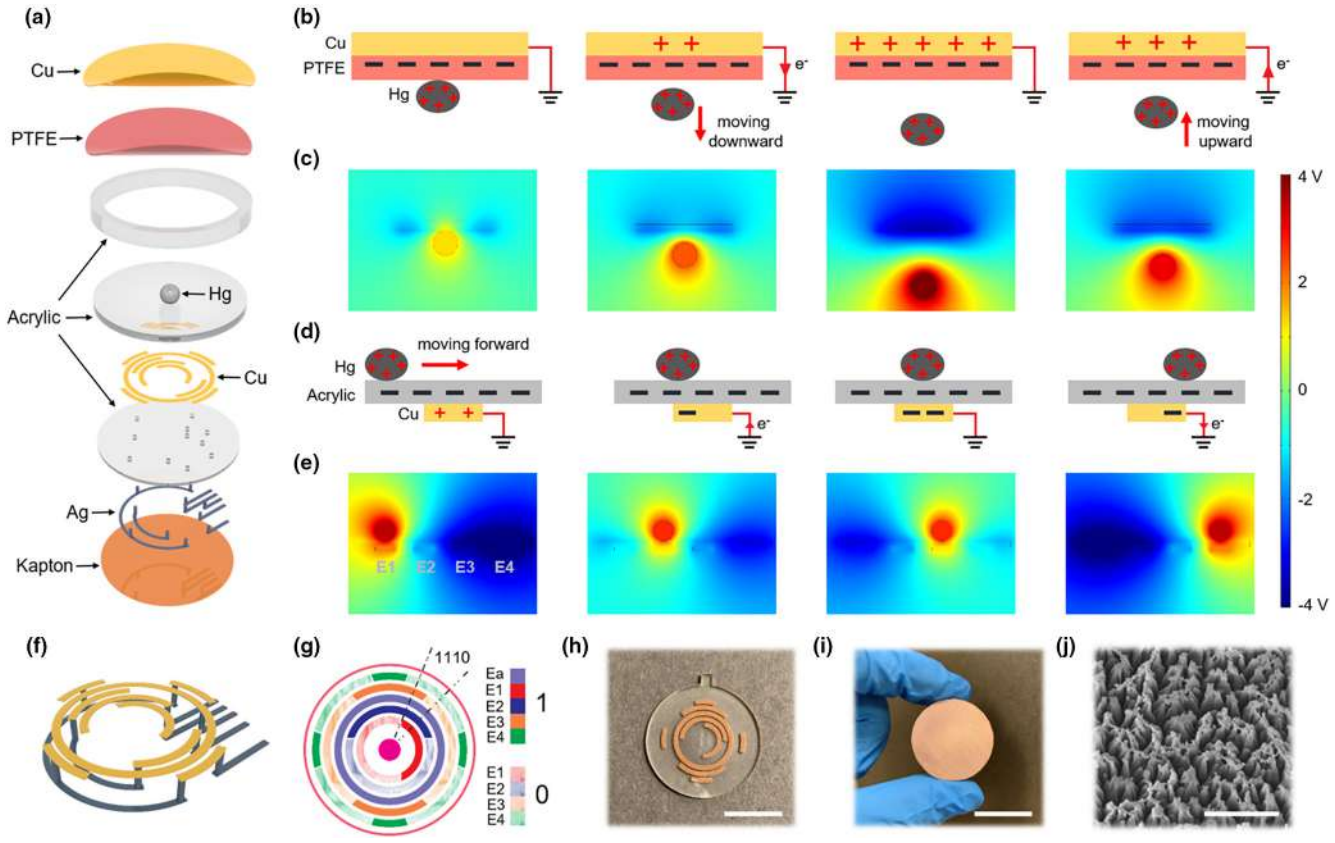

FIGURE 1

Structural design and working principle of the coded liquid metal 3D acceleration sensor. (a) Schematic representation of the 3D acceleration sensor. (b) Working process of the 3D acceleration sensor to detect the vibration in vertical. (c) Numerical calculations on the potential distribution between the Hg droplet and PTFE film with the Hg droplet moving up and down. (d) Working mechanism of the 3D acceleration sensor vibrating in the horizontal direction. (e) Potential distribution between the Hg droplet and the substrate with the Hg droplet moving from the inner electrode (E1) to the outer electrode (E4). (f) The connection method of the Copper electrode and the silver electrode. (g) Schematic illustration of the copper electrode distribution in (f) and the coded strategy of the four electrodes (E1–E4) used to detect the movement direction in horizontal. Ea is the electrode to detect the acceleration in the horizontal direction. (h) Digital photograph of the coded electrode. Scale bar, 1.5 cm. (i) Photograph of the 3D acceleration sensor. Scale bar, 2 cm. (j) SEM image of the PTFE surface with nanowires modification. Scale bar, 2 μm.

ball are chosen to be the moving part. Ascribing to the outstanding properties of liquid metal, such as high electrical conductivity, high solid–liquid interfacial tension, high elasticity as well as high energy conversion efficiency, the open-circuit voltage of mercury droplet is much higher than that of the water droplet and PTFE ball. The contact angles of the mercury and water droplets on the surface of acrylic are clearly displayed in Fig. 2b, indicating that the surface tension of mercury is much larger than that of the water. Moreover, the water droplet can be easily broken into pieces and possibly form a thin water layer that reduces triboelectric charge density. PTFE ball is not suitable in this case either, owing to the vertical triboelectric layer is also PTFE. The accuracy of acceleration detection in the horizontal direction is mainly depended on the structure design of the electrodes. As shown in the Fig. 2c, d and S5, the open-circuit voltage of the four electrodes are influenced by the distance between the mercury droplet and the edge of the electrodes, where d is the distance between the center of the droplet and the edge of the electrode. As clearly demonstrated in Fig. 2d, the open-circuit voltage decreases with the increase of the distance d. The output voltage when the droplet moves above the electrode is much larger than that when the droplet moves at the side of the electrodes, indicating that the accuracy of the direction identification is very high based on the coded electrodes. The relationship between the features of the voltage waveforms and the motion position is demonstrated in Fig. S6. The normal coded strategy is composed of four half-circled electrodes which can distinguish sixteen directions, as shown in Fig. 2e. However, the volume of the mercury droplet cannot be ignored in the actual operation process. As clearly demonstrated in Fig. 2g and h, when the droplet moves in the direction of 0111 and 1001, because of the volume effect of the droplet, it contacts with the electrode 1 and electrode 2 respectively, as a result, the identified results will shift to be 1111 and 1101. In the other situation, when the droplet moves along the direction of 1100, the detected direction can be 1111 for the same reason, as demonstrated in Fig. S7. Hence, the length of the coded electrodes must be reduced to avoid the volume effect of the liquid metal droplet to further enhance the accuracy of direction identification. As shown in Fig. 2f, the length of the electrodes is reduced according to the actual running path of the droplet. With the improved coded electrodes, the accuracy of direction identification of the

Please cite this article in press as: B. Zhang et al., Materials Today (2020), https://doi.org/10.1016/j.mattod.2020.10.031

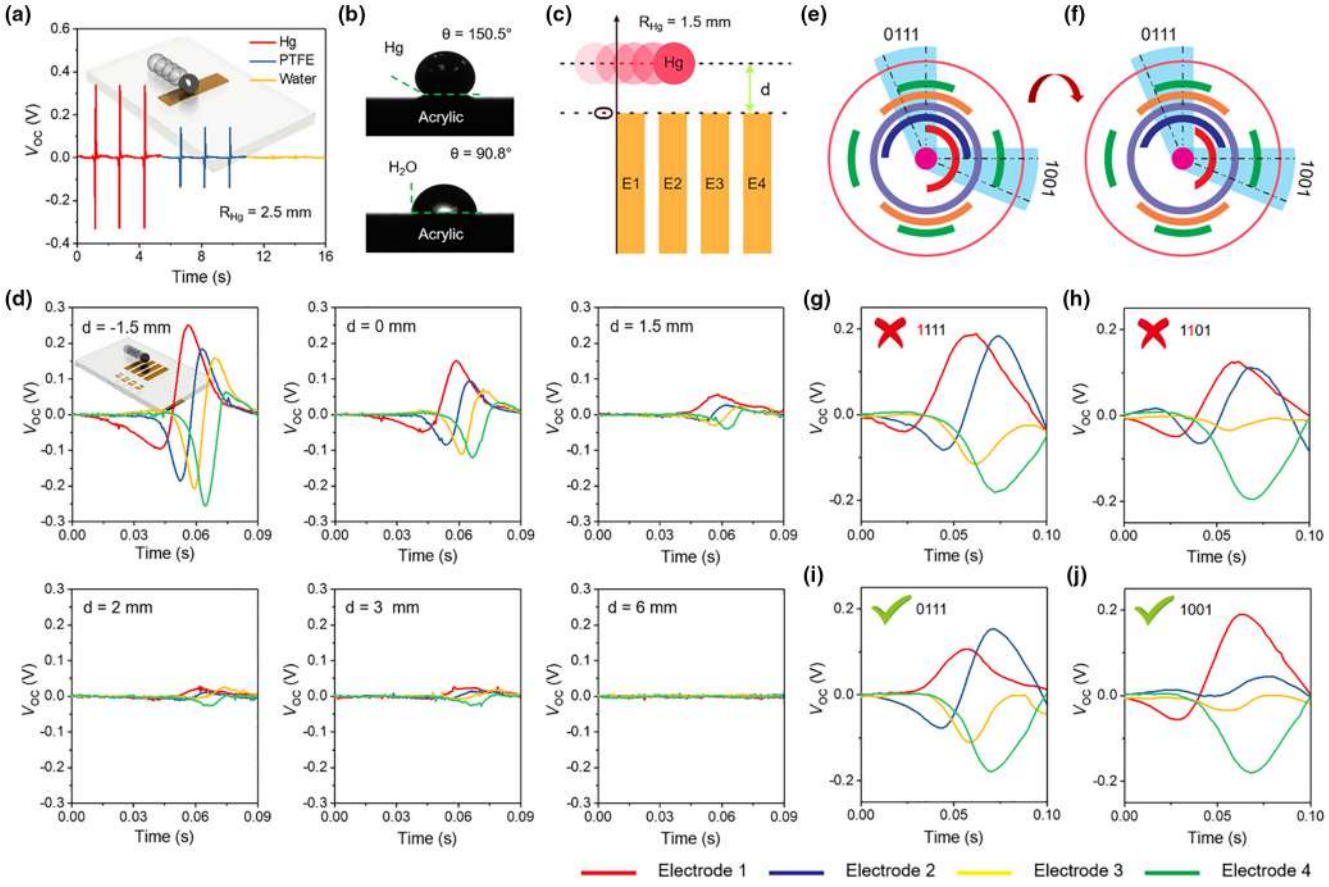

FIGURE 2

Materials selection and the structure design of the coded liquid metal 3D acceleration sensor. (a) Open-circuit voltage generated by a different types of ball (Hg, PTFE and Water) moving across the copper electrode, in which both the diameter of the ball and the width of the electrode are 5 mm. (b) Contact angle of the Hg and water on the surface of acrylic. (c) Schematic diagram of the test process when the Hg droplet moves from electrode E1 to E4 with different distance between Hg droplet and the electrode, in which the diameter of Hg droplet is 3 mm and the width of the electrodes is 2 mm. (d) Open-circuit voltage of the four electrodes with the Hg droplet moving from electrode E1 to E4 with d ranging from −1.5 mm to 6 mm. (e and f) Electrode pattern in normal coded method (e) and improved coded method (f). (g and h) Open-circuit voltage of the sensor with the Hg droplet moving in the direction of 0111 (g) and 1001 (h) with normal coded method. (i and j) Open-circuit voltage of the sensor with the Hg moving in the direction of 0111 (i) and 1001 (j) with improved coded strategy.

sensor is significantly improved, as shown in Fig. 2i, j, and S7. The schematic illustration of the transformation of the length of the electrodes and the coded strategy are clearly shown in Fig. S8 and S9.

The direction identification of the sensor in the horizontal direction is illustrated in Fig. 3. In the testing progress, the AS is mounted on a linear motor, where the moving acceleration and distance of the motor are fixed. When the motor moves forward, the sensor also moves in the same direction, meanwhile, due to the inertia, the droplet moves in the opposite direction. There is a trough occurred on the tested voltage curve when the droplet moves across the corresponding electrode (1), conversely, there is a crest or nothing occurred on the curve (0). As clearly illustrated in Fig. 3a, the typical feature of the voltage waveform on the electrodes from E1 to E4 can be classified into two areas, the inertia movement area (state I) and the reciprocating movement area (state II), when the liquid metal droplet moves in the direction of 1111. The force and movement analysis of the mercury droplet in the different situations is respectively demonstrated in Fig. 3b. When a force (F) applied to the acceleration sensor in the horizontal direction, because of the inertia force (F_1), the mercury droplet moves in the opposite direction until knocks to the acrylic ring (state I). At this moment, the thrust (F_2 and F_3) and gravity (G) drive the droplet return to the center of the substrate automatically after several times of reciprocating movement, owing to that the acrylic substrate is designed in a concave shape (state II). The schematic diagrams for the definitions of the 16 directions identified by the sensor with four coded electrodes are shown in Fig. S10. The acceleration direction can be identified in a high accuracy according to the voltage waveform of the electrodes from E1 to E4, as shown in Fig. 3c-h, and the other direction identification results are demonstrated in Fig. S11 and S12 respectively.

As a 3D AS, it is necessary to investigate the relationship between the electric output and acceleration. A ring-shaped electrode is utilized to detect the acceleration in the horizontal direction, where the time from 0 to the trough of the open-circuit voltage curve is captured. As shown in Fig. 4a, the duration follows an exponential decay when the acceleration increase from 1 to 100 m/s^2, moreover, the experimental data is fixed well with

Please cite this article in press as: B. Zhang et al., Materials Today (2020), https://doi.org/10.1016/j.mattod.2020.10.031

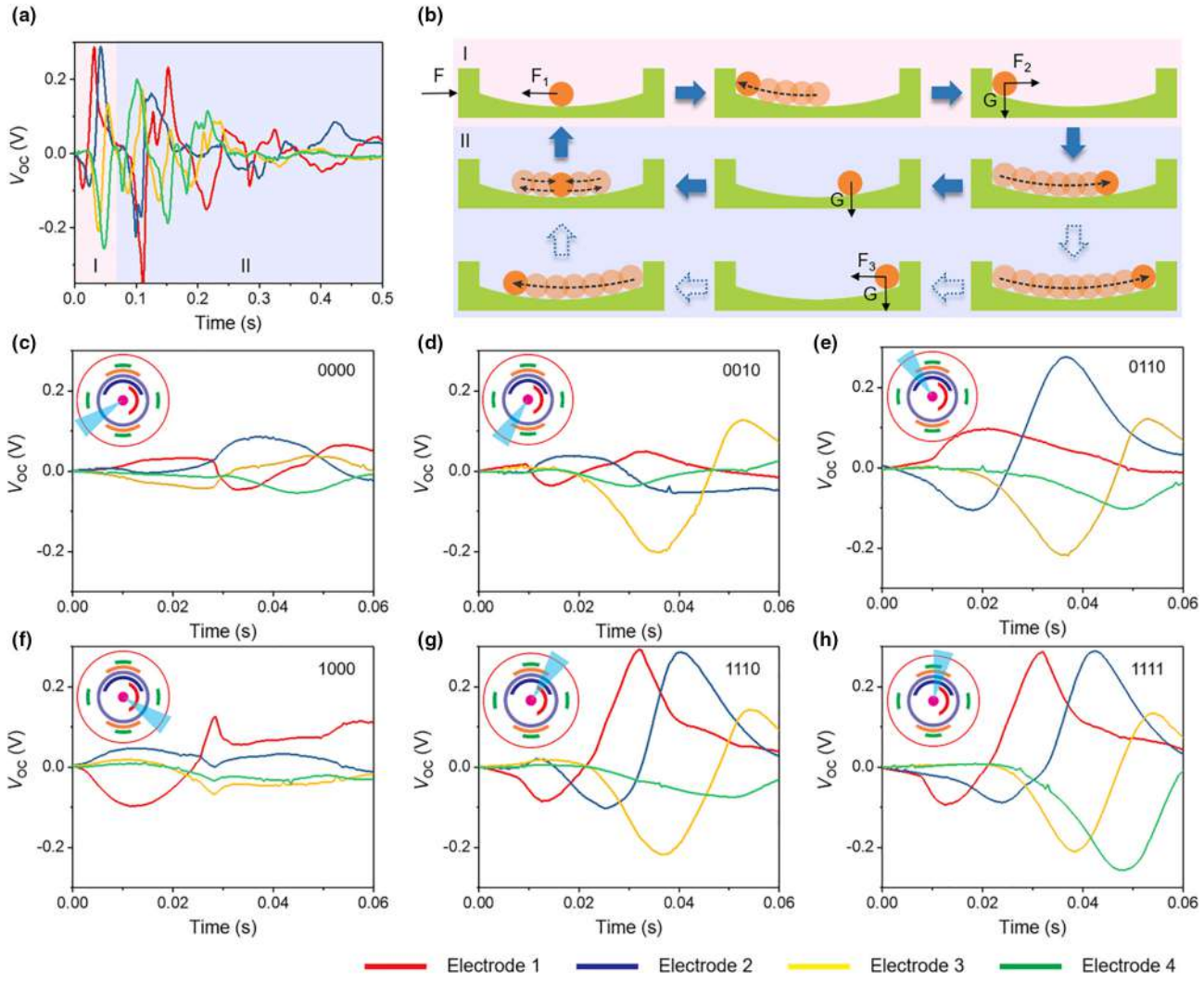

FIGURE 3

Acceleration measurement in the horizontal direction of the 3D acceleration sensor based on liquid metal. (a) Open-circuit voltage of the four electrodes when a specific force applied to the sensor in the direction of 0011. (b) Force and movement analysis of the Hg droplet when an external stimulation applied to the sensor. (c–h) Open-circuit voltage of the sensor with the moving direction of the Hg droplet ranging from 0000 to 1111. (c) 0000, (d) 0010, (e) 0110, (f) 1000, (g) 1110, (h) 1111.

the fitted curve. The response time of the sensor at various accelerations is demonstrated in Table S2. The open-circuit voltage of the sensor at variable accelerations of 5, 10, 20, 50 and 100 m/s^2 is illustrated in Fig. 4b. The acceleration of the sensor is also detected when the sensor moves in several directions with a fixed acceleration, as demonstrated in Fig. 4c, indicating that the sensor possesses high accuracy in the detection of acceleration in the horizontal direction. When the 3D AS is subjected to a certain external acceleration in the Z-axis, the electricity will be generated ascribing to the contact and separation between the mercury droplet and the PTFE film as a single- electrode TENG. As shown in Fig. 4d, the open-circuit voltage of the acceleration sensor is proportional to the external vibration acceleration in a wide range from 0 to 50 m/s^2. At the acceleration of 50 m/s^2, the open-circuit voltage can reach up to 4 V with a sensitivity of 800 mV/g. The acquired open-circuit voltage of the sensor at variable accelerations of 10, 20, 30, 40 and 50 m/s^2 is demonstrated in Fig. 4e and the mean value and standard deviation of voltage are demonstrated in Table S3. To have a deeper comprehension of the progress, the COMSOL is utilized to calculate the potential distribution for different contact area between the droplet and PTFE film, as shown in Fig. S13 and supporting movie 3. It is clearly indicated that the potential difference increases with the increase of the contact area. As we know, the contact area between the droplet and the film is mainly determined by the acceleration of the droplet, hence, there will be a linear relationship between the open-circuit voltage and the acceleration of the droplet. As shown in Fig. 4f, the 3D acceleration sensor can measure vector acceleration in three-dimensional space by calculating the two acceleration data, in which, the red points represent the actual vector accelerations and the blue point represent the measured accelerations. The maximum error of the measured acceleration is 1.5 m/s^2, which is within the standard deviation range. Furthermore, the stability and durability test of the acceleration sensor is carried out at the acceleration of 10 m/s^2 in the horizontal direction and 20 m/s^2 in the vertical

Please cite this article in press as: B. Zhang et al., Materials Today (2020), https://doi.org/10.1016/j.mattod.2020.10.031

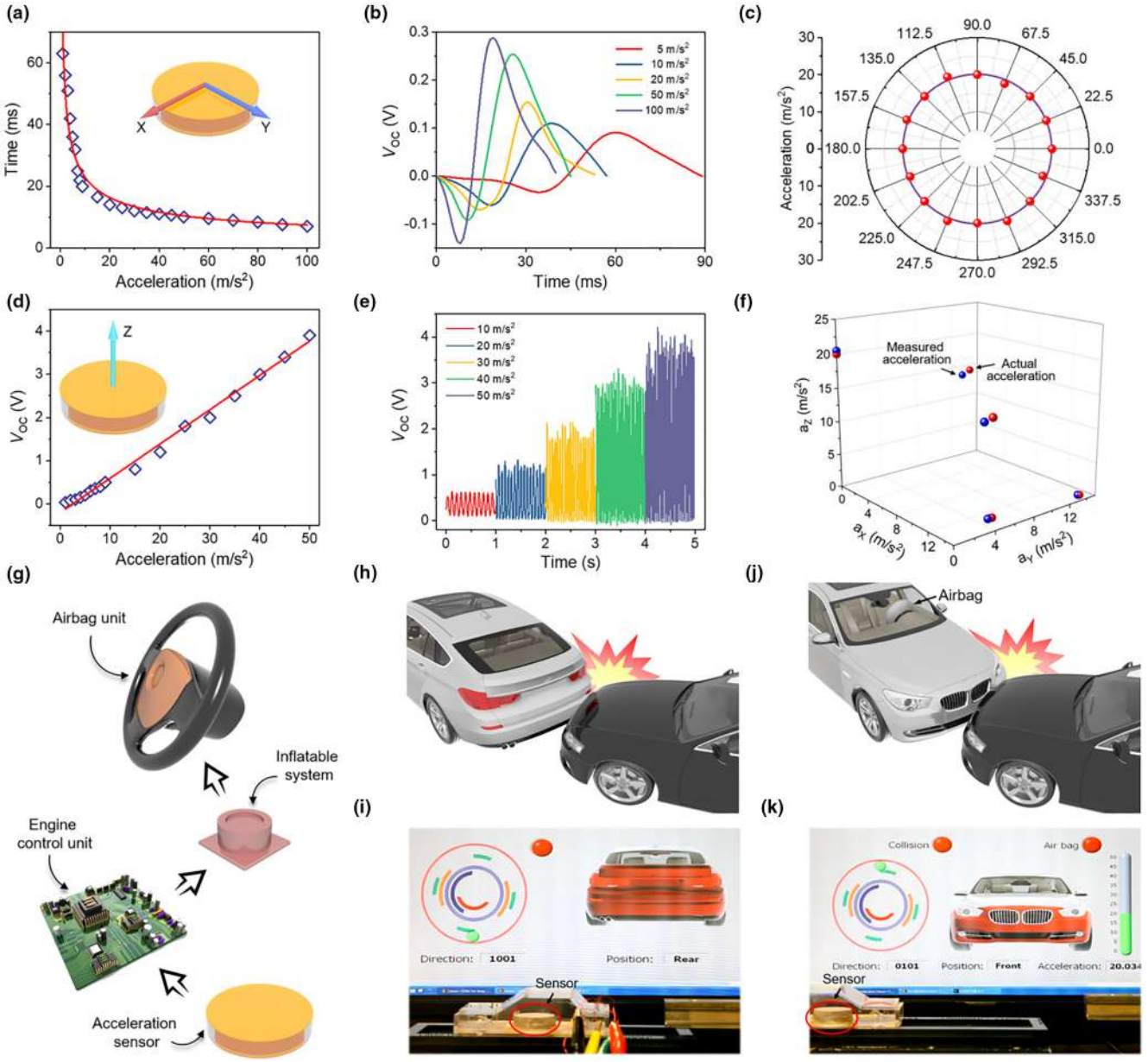

FIGURE 4

Acceleration measurement in full space of the 3D acceleration sensor and its application in the vehicle safety restraint system. (a) Dependence of the time from 0 to the trough of the open-circuit voltage on the loaded acceleration in the horizontal direction. (b) Open-circuit voltage of the sensor at variable accelerations ranging from 5 to 100 m/s^2. (c) Detected acceleration with the sensor moving in different direction with a fixed acceleration of 20 m/s^2. (d) Dependence of the open-circuit voltage of the sensor on the loaded acceleration in the vertical direction. (e) Open-circuit voltage of the sensor at variable accelerations ranging from 10 to 50 m/s^2. (f) Acceleration measurement in the 3 dimensional direction. (g) Schematic representation of the working process of the vehicle safety restraint system. (h and i) Collision position of the vehicle detected by the 3D acceleration sensor (rear position). (j and k) Collision position and force detected by the sensor, which can provide information to the vehicle safety restraint system (front position).

direction. As shown in Fig. S14, after 1800 continuous operation in the horizontal direction and 100,000 vibration cycles in the vertical direction, the open-circuit voltage exhibits only negligible drops, indicating high durability of the acceleration sensor, owing to that the liquid–solid contact of mercury droplet and acrylic or PTFE film reduces the abrasion of the nanostructures. To prove the capability of the 3D AS based on LM-TENG as a part of the vehicle restrain systems, a collision experiment is simulated, as schematically illustrated in Fig. 4g. When a collision accident happens to a vehicle, the impact acceleration is measured by the sensor and determined whether and when to deploy the airbag. As shown in Fig. 4h, i and supporting movie 4, the acceleration sensor embedded in the car can identify the collision position of the vehicle efficiently. Then, as clearly shown in Fig. 4j, k and supporting movie 5, the collision position is controlled to the front and the impact acceleration alters from a low value to a high value, the acceleration sensor can efficiently measure the impact acceleration and identify the collision position in order to determine whether the airbag should be deployed to protect the safety of the occupants. This prototype of a LM-

Please cite this article in press as: B. Zhang et al., Materials Today (2020), https://doi.org/10.1016/j.mattod.2020.10.031

TENG-based 3D AS shows the potential for creating a sensitive and effective commercial sensor for vehicle safety restraint systems.

Conclusion

In summary, a self-powered active 3D acceleration sensor based on liquid metal triboelectric nanogenerator was demonstrated with features of small size, lightweight, low-cost, high integration, high sensitivity, large detection range and excellent stability. The accuracy of the acceleration sensor has been significantly improved by eliminating the volume effect of liquid metal. Due to the nanowires structure of PTFE film and inherent characteristic of the liquid metal, the acceleration sensor exhibits high sensitivity and excellent stability. The relationship between the electric output properties and the applied acceleration is theoretically and experimentally investigated. Furthermore, the 3D acceleration sensor is utilized to be a part of the vehicle safety restraint system to measure the collision position and force. This work not only demonstrates a self-powered 3D acceleration sensor but also expands TENG's commercialization and application in self-powered sensing systems.

Experimental section

Fabrication of the nanowire structures on the surface of the PTFE thin film

A 30 μm thick PTFE thin film was cleaned with ethyl alcohol and ultra-pure water, consecutively, and then dried by compressed air. A thin Au film (10 nm) was deposited on the PTFE surface with a deposition rate of 0.2 nm s^{-1} by using a Denton Explorer E-beam Evaporator. The nanowires structure on the PTFE surface was created by ICP reactive ion etching. The flow rates of the Ar, O_2, and CF_4 gases are 15, 10, and 30 sccm, respectively. One power source of 400 W was used to generate a high density of plasma, while another 100 W was used to accelerate the plasma ions.

Fabrication of the acceleration sensor

A 1.5 mm thick acrylic sheet was cut into a disk (D_1) with a diameter of 29 mm, then a pit with a slope angle of nearly 5 degrees was engraved by the laser cutter (Universal Laser System, PLS6.75). On the other side of the disk, the patterned copper electrodes (200 nm in thickness, 1 mm in the width) were deposited by using a Denton Explorer E-beam Evaporator. Next, a 1.5 mm thick acrylic disk (D_2) (29 mm in diameter) with several hole channels (0.8 mm in diameter) cut by the laser cutter was attached on the electrode side of the D_1. Silver conductive epoxy (component A and B was mixed by 1:1) was used to form the test electrodes. Then, a Kapton film (30 μm in thickness) was stuck on the back of D_2. A ring-shaped acrylic with an outer diameter of 29 mm, inner diameter of 27 mm and a height of 1.7 mm was fabricated by the laser cutter. Then, it was attached on the D_1 to limit the movement of the mercury ball. A 200 nm thick copper film was deposited on the PTFE film by a Denton Explorer E-beam Evaporator. Finally, a mercury droplet was added into the pit of the acrylic shell, and a tailored PTFE film was attached onto the acrylic substrate. For the packaging of the device, the acrylic plates were firmly connected with each other by the Loctite 414 and the PTFE film and the acrylic substrate were tightly bonded by the VHB tape (3 M Company). After that, the epoxy resin was coated on the outer surface of the device to further enhance the tightness and safety of the acceleration sensor.

Measurement of the LM-TENG

The TENG was mounted on a linear motor (LinMot H01-23 × 86/160) and the moving distance and acceleration can be controlled by the linear motor. The open-circuit voltage was measured by using a Keithley 6514 system electrometer and a data acquisition device (National Instruments, BNC-2120).

CRediT authorship contribution statement

Binbin Zhang: Conceptualization, Methodology, Data curation, Investigation, Writing - original draft, Writing - review & editing. **Zhiyi Wu:** Methodology, Visualization, Data curation, Investigation, Writing - original draft, Writing - review & editing. **Zhiming Lin:** Methodology, Data curation, Investigation, Writing - original draft, Writing - review & editing. **Hengyu Guo:** Data curation, Investigation. **Fengjun Chun:** Methodology, Investigation. **Weiqing Yang:** Visualization, Investigation. **Zhong Lin Wang:** Supervision, Conceptualization, Writing - original draft, Writing - review & editing.

Declaration of Competing Interest

The authors declare that they have no known competing financial interests or personal relationships that could have appeared to influence the work reported in this paper.

Acknowledgements

The authors are grateful for the support received from the Hightower Chair Foundation. Miaozi Project of Sichuan province (2019015), Cultivation Program for the Excellent Doctoral, Dissertation of Southwest Jiaotong University.

Appendix A. Supplementary data

Supplementary data to this article can be found online at https://doi.org/10.1016/j.mattod.2020.10.031.

References

[1] L. Jin et al., Nano Energy 38 (2017) 185.
[2] M.R. Elliott et al., Arch. Pediatr. Adolesc. Med. 160 (2006) 617.
[3] L. Jin et al., Nano Energy 66 (2019) 104086.
[4] Y. Pang et al., ACS Appl. Mater. Interfaces 7 (2015) 19076.
[5] A.L. Roy et al., Sens. Actuators, A 210 (2014) 77.
[6] Z. Shen et al., Sens. Actuators, A 241 (2016) 113.
[7] L. Jin et al., Nano Energy 50 (2018) 632.
[8] C. Xu et al., Adv. Mater. 30 (2018) 1803968.
[9] Z. Lin et al., Nano Energy 64 (2019) 103908.
[10] L. Zhang et al., Adv. Mater. 28 (2016) 1650.
[11] W. Liu et al., Nat. Commun. 10 (2019) 1426.
[12] Y. Liu et al., Nat. Commun. 11 (2020) 1599.
[13] W. Liu et al., Nat. Commun. 11 (2020) 1883.
[14] W. He et al., Nat. Commun. 11 (2020) 4277.
[15] L. Jin et al., Acs Nano 10 (2016) 7874.
[16] Z. Lin et al., Adv. Mater. Technol. 4 (2019) 1800360.
[17] Z. Wu et al., Acs Nano 12 (2018) 5726.
[18] J. Wang et al., Acs Nano 13 (2019) 2587.
[19] B. Zhang et al., Acs Nano 10 (2016) 6241.
[20] H. Guo et al., Sci. Rob. 3 (2018) eaat2516.
[21] X. Pu et al., Sci. Adv. 3 (2017) e1700015.
[22] Z. Wen et al., Nano Energy 16 (2015) 38.

Please cite this article in press as: B. Zhang et al., Materials Today (2020), https://doi.org/10.1016/j.mattod.2020.10.031

[23] C. Wu et al., Mater. Today 21 (2018) 216.
[24] Y. Wu et al., Adv. Funct. Mater. 25 (2015) 2166.
[25] B. Zhang et al., Acs Nano 11 (2017) 7440.
[26] W. Tang et al., Adv. Funct. Mater. 25 (2015) 3718.
[27] Y. Chen et al., Mater. Horiz. 4 (2017) 591.
[28] H. Zou et al., Nat. Commun. 10 (2019) 1427.
[29] Z.L. Wang, Nano Energy 68 (2020) 104272.
[30] Z. Lin et al., Nano Energy 68 (2020) 104378.

Please cite this article in press as: B. Zhang et al., Materials Today (2020), https://doi.org/10.1016/j.mattod.2020.10.031